Desalination and Water Treatment
www.deswater.com
51 (2013) 1242–1253
January
1944-3994/1944-3986 © 2013 Desalination Publications. All rights reserved
doi: 10.1080/19443994.2012.695044
Taylor & Francis
Taylor & Francis Group

Numerical simulation of solar-assisted multi-effect distillation (SMED) desalination systems

Young-Deuk Kim[a], Kyaw Thu[a], Aung Myat[b], Kim Choon Ng[b,*]

[a]*Water Desalination and Reuse Center, 4700 King Abdullah University of Science and Technology, Thuwal 23955-6900, Saudi Arabia*
[b]*Department of Mechanical Engineering, National University of Singapore, 10 Kent Ridge Crescent, Singapore 117576, Singapore*
Tel. +65 6516 2214; email: mpengkc@nus.edu.sg

Received 11 March 2012; Accepted 10 May 2012

ABSTRACT

We present a simulation model for the transient behavior of solar-assisted seawater desalination plant that employs the evacuated-tube collectors in conjunction with a multi-effect distillation plant of nominal water production capacity of 16 m^3/day. This configuration has been selected due to merits in terms of environment-friendliness and energy efficiency. The solar-assisted multi-effect distillation system comprises 849 m^2 of evacuated-tube collectors, 280 m^3 water storage tanks, auxiliary heater, and six effects and a condenser. The present analysis employs a baseline configuration, namely; (i) the local solar insolation input (Jeddah, Saudi Arabia), (ii) a coolant flow rate through the headers of collector based on ASHRAE standards, (iii) a heating water demand, and (iv) the augmentation of water temperature by auxiliary when the supply temperature from the solar tank drops below the set point. It is observed that the annual collector efficiency and solar fraction decrease from 57.3 to 54.8% and from 49.4 to 36.7%, respectively, with an increase in the heating water temperature from 80 to 90°C. The overall water production rate and the performance ratio increase slightly from 0.18 to 0.21 kg/s and from 4.11 to 4.13, respectively.

Keywords: Desalination; Evacuated-tube collector; Multi-effect distillation; Mathematical modeling; Numerical simulation

1. Introduction

Man-made desalination processes are both energy-intensive and environment polluting as they consumed thermal energy, electricity, and chemicals in separating the dissolved salts from saline or brackish water. Schematically, such a desalination process is summarized as Fig. 1, where the saline or brackish feed is fed into a desalination process with the simultaneous consumption of energy and chemicals to produce the distillate that is suitable for human consumption while emitting heat, carbon dioxide, and discharging chemically laden brine to the environment. Table 1 shows the comparison of energy (electricity and thermal energy) consumption in kWh/m^3

*Corresponding author.

Presented at the International Conference on Desalination for the Environment, Clean Water and Energy, European Desalination Society, 23–26 April 2012, Barcelona, Spain

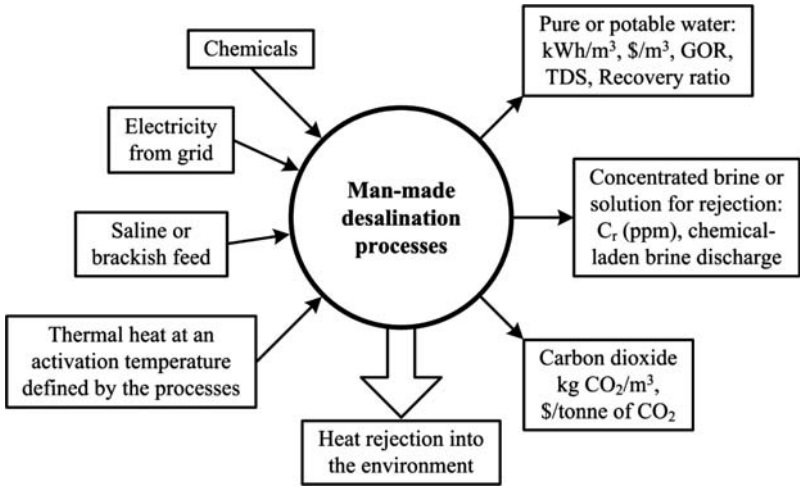

Fig. 1. A schematic of a man-made desalination process that consumes energy and chemicals to yield potable or pure water.

Table 1
A comparison of the costs for various desalination methods [1]

	Consumption of electrical energy (kWh/m^3)	Consumption of thermal energy (kWh/m^3)	Temperature level of the thermal energy (°C)
MSF (electrical motors as pump drivers)	3.5	50	120
MSF (back-pressure turbine as recirculation pump drive)	1.0	52	120
ME	1.0	40–70	70
ME-TVC	1.0	40–70	200
ME-MVC	8.0–12.0	N.A.	N.A.
RO	5.0–7.0	N.A.	N.A.
AD	1.38 [2]	Waste heat [3]	50–85 [4]

of water for various desalination methods widely used in the world.

In an attempt to be environment-friendly and yet minimize the energy input to the desalination process, we analyze the solar-assisted desalination cycle, which is coupled with a multi-effect distillation (MED). The MED cycle is chosen over the multi-stage flashed (MSF) due to the lower top-brine-temperature (TBT), typically less than 80°C. Recent literature, such as the multi-stage flash distillation (MSF) [5], MED [6], and reverse osmosis (RO) driven by the photovoltaic solar cells [7], have reported the efficacy of the solar-assisted concept, the MED hybrids have better attributes in terms of specific energy consumption as well as less susceptible corrosion and scaling. This is mainly due to the lower TBT of MEDs. Secondly, the lower TBT makes the MED plants suitable for integration with solar energy where cost-effective and stationary thermal collectors, such as the evacuated-tube collectors (ETC), could be used to meet the TBT requirement. The key consideration here is the maximum collection of thermal energy, above that of a designed threshold or useful temperature, by thermal collectors rather than the maximum achievable temperature supplied to the MED plants. Several investigations of the dependence of MED process on the solar collector systems have been conducted.

In this study, we focus on the long-term thermal and performance analyses based on the numerical simulation of a solar-assisted multi-effect distillation (SMED) system. A numerical model along with the simulation has developed to predict the transient behavior of a solar-powered seawater desalination plant that utilizes an ETC coupled with a backward-feed type MED system. The SMED system comprises 849 m^2 of evacuated-tube collectors, 280 m^3 water stor-

age tanks, auxiliary heater (pre-set to supply hot water at a TBT), and six effects. The baseline data for SMED are: (i) the local solar insolation input (Jeddah, Saudi Arabia), (ii) a coolant flow rate through the headers of collector based on the ASHRAE standards, (iii) a pre-set heating water demand, and (iv) the dynamic augmentation of water temperature by auxiliary when the supply temperature from the solar tank drops below the set point. The system performance is reported in terms of the annual solar fraction and collector efficiency, as well as the overall water production rate and performance ratio.

2. Model description

A schematic diagram of an SMED system is shown in Fig. 2. The SMED system comprises solar-thermal and MED systems. The solar-thermal system has two circuits i.e., the primary solar circuit for the collection of solar energy and the secondary circuit that circulates the hot water among the four solar hot water tanks. These two circuits are thermally communicated via a plate heat exchanger. The four storage tanks are constructed in a top-to-bottom arrangement to achieve thermal stratification yet fulfill the thermal demand of the load in terms of hot water supply. The hot water from storage tank-1 is supplied to the first effect of the MED system, while the inline heater is installed as a supplementary heater to maintain the temperature of the heat source. The return hot water is sent back to the tanks dynamically based on the temperature, i.e. it is supplied to the tank with temperature closest to but less than that of the return hot water. It is noted that the hot water mass flow rate withdrawn from the storage tank-1 is equal to the desired load flow rate, regardless of the storage temperature. Whenever the storage tank-1 temperature falls below the desired load temperature, the maximum possible portions of the energy demand are supplemented by keeping the discharge mass flow rate equal to the desired load flow rate and the rest of the energy demand being supplied by the auxiliary. The primary pump's operation is controlled based on the collector outlet temperature and the inlet temperature of the plate heat exchanger in the secondary circuit. It is activated whenever the temperature of the primary pump is higher than that of the plate heat exchanger.

In the MED system, there is a backward-feed arrangement where the feed seawater enters the last stage (the condenser), and the feed is progressively heated to the boiling temperature in next effect. Part of the feed is evaporated utilizing the heat gained by condensing the vapor coming from the preceding effect. The brine leaving last effect is pumped to the preceding effect as feed and so on. The hot brine leaving the TBT or the first effect is fed to a heat exchanger before being thrown back to the sea. Thus, the feed and vapor entering the effects have opposite flow directions. The brine salinity and temperature are highest at the first effect and lowest at the last effect.

2.1. Solar radiation

For the local solar insolation input, the monthly average hourly global radiation incident upon a tilted surface is estimated with several existing empirical theories, based on the monthly average daily global radiation ($MJ/m^2/day$) with the 22-year average data of the NASA SSE model [8]. Here, the global radiation consists of beam and diffuse com-

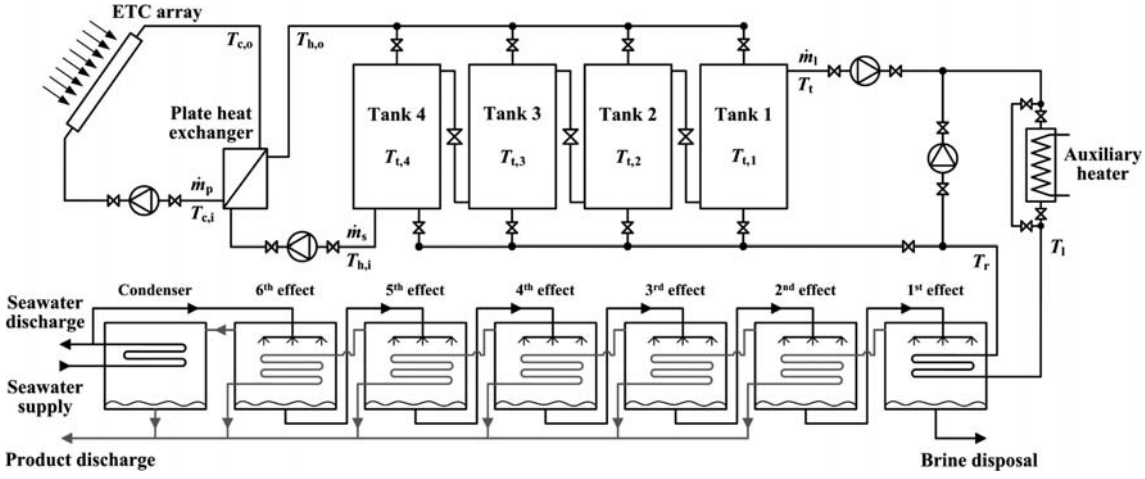

Fig. 2. Schematic of solar assisted multi-effect distillation (SMED) system.

ponents. The monthly average daily diffuse and beam radiations on a horizontal surface are based on the measured monthly average daily global radiation, while the monthly average daily diffuse radiation is calculated from the monthly average diffuse fraction correlation. They are expressed as a function of the monthly average clearness index and sunset (or sunrise) hour angle [9]. The monthly average daily diffuse and global radiations on a horizontal surface are then converted into the monthly average hourly diffuse and global radiations by means of the ratio of hourly global to daily global radiation, as a function of the day length and the hour in question [9,10]. To estimate the monthly average hourly global irradiation on a tilted surface, Hay–Davies–Klucher–Reindl (HDKR) diffuse model, which takes into account the circumsolar diffuse and horizon brightening components on a tilted surface, is used. Hay and Davies [11] estimated the fraction of the diffuse that is circumsolar and considered it to be all from the same direction as the beam radiation, but they did not consider horizon brightening. Temps and Coulson [12] accounted for horizon brightening on clear days by applying a correction factor of $[1+\sin^3(\beta/2)]$ to the isotropic diffuse. Klucher [13] modified this correction factor by a modulating factor so that it has the form $[1+f\sin^3(\beta/2)]$ to account for the cloudiness. Reindl et al. [14] modified the Hay and Davies [11] model by the addition of a term like that of Klucher [13], giving a model to be referred to as the HDKR diffuse model. The diffuse on the tilted surface is

Table 2
Plant parameters and input data for the SMED system

Location	Latitude, ϕ (° North)	21.67
	Longitude, L_{loc} (° East)	39.15
Load	Heating water temperature, T_l (℃)	80, 85, 90
	Heating water flow rate, $\dot{m}_l$ (kg/s)	5.5
Solar collector	Evacuated-tube collector (HP 200 30), Thermomax Ltd.	
	Total collector area, A_c (m^2)	849
	Aperture area per collector, A_a (m^2)	3.229
	Number of tubes per collector	30
	Number of collectors in series	1
	Optical efficiency, η_0	0.727
	Global heat loss coefficient, c_1 ($W/m^2℃$)	0.85
	Temperature dependence of global heat loss coefficient, c_2 ($W/m^2℃^2$)	0.0,093
	Effective thermal capacity, c_3 (kJ/m^2K)	4.2
	Tilt angle, β (°)	20
	Azimuth angle, γ (°)	0
	Mass flow rate per unit area of collector, G (kg/m^2s)	0.02
Storage tank	Cylindrical, always full, with (H/D) = 2.5	
	Volume, V_t (m^3)	280
	Heat loss coefficient, U ($W/m^2℃$)	1.5
Plate heat exchanger	Single-pass ($N_{pass}=1$), U-type counterflow arrangement	
	Effective plate length, L_h (m)	1.5
	Effective plate width, L_w (m)	0.5
	Chevron angle, D (°)	45
	Plate pitch, p (m)	3.5×10^{-3}
	Plate thickness, t (m)	6.0×10^{-4}
	Enlargement factor, ϕ	1.17
	Fouling factor, R_f (m^2 ℃/W)	1.7×10^{-4}
	Thermal conductivity of plate (SS316), k_p ($W/m℃$)	14.6
Multi-effect distillation	Seawater temperature to condenser, $T_{f,in}$ (℃)	30
	Seawater concentration, $X_{f,in}$ (ppm)	35,000
	Total area of the effects, $A_{e,o}$ (m^2)	250.8
	Condenser area, $A_{c,o}$ (m^2)	7.9
	Seawater flow rate to condenser, $\dot{m}_{f,in}$ (kg/s)	3.15

$$I_{d,T} = I_d\left\{(1-A_i)\left(\frac{1+\cos\beta}{2}\right)\left[1+f\sin^3\left(\frac{\beta}{2}\right)\right]+A_iR_b\right\} \quad (1)$$

where A_i (=I_b/I_o) is an anisotropic index which is a function of the transmittance of the atmosphere for beam radiation and $f=(I_b/I_h)^{1/2}$.

The total radiation on the tilted surface is then

$$I_T = (I_b + I_dA_i)R_b + I_d(1-A_i)\left(\frac{1+\cos\beta}{2}\right) \times\left[1+f\sin^3\left(\frac{\beta}{2}\right)\right]+I_h\rho_g\left(\frac{1-\cos\beta}{2}\right) \quad (2)$$

where the geometric factor R_b (=$\cos\theta/\cos\theta_z$) is the ratio of beam radiation on the tilted surface to that on a horizontal surface at any time.

The procedure for estimating the solar radiation incident upon a tilted surface is discussed in more detail by Kim et al. [15].

2.2. Evacuated-tube collector

The collector efficiency is defined as the ratio between the useful energy delivered over the aperture area and the total irradiance of the collector aperture, according to Rabl [16]:

$$\eta = \frac{q_u}{A_aG_T} = \frac{\dot{m}_pc_{p,c}(T_{c,o}-T_{c,i})}{N_cA_aG_T} \quad (3)$$

The efficiency curve provided by the manufacturer is obtained from efficiency tests according to the standard [17]. The efficiency curve is described after a second degree fit of efficiency points measured at different collector temperatures and follows from:

$$\eta = \eta_0 - c_1\frac{T_m-T_a}{G_T} - c_2G_T\left(\frac{T_m-T_a}{G_T}\right)^2 \quad (4)$$

with $T_m=(T_{c,i}+T_{c,o})/2$.

Since the efficiency curve is produced on the basis of normal incidence measurements, its use for different incident angles requires the correction of the optical efficiency, measured at normal incidence, by the appropriate incident angle modifier for beam and diffuse irradiances. Thus, the collector efficiency at any incidence angle is calculated as:

$$\eta(\theta) = \eta_0K_{\theta b}(\theta) + \eta_0K_{\theta b} - c_1\frac{T_m-T_a}{G_T} - c_2G_T\left(\frac{T_m-T_a}{G_T}\right)^2 \quad (5)$$

with $K_{\theta b}(\theta)$ being a function of the incidence angle of beam irradiance and the constant $K_{\theta d}$ for the diffuse irradiance. Here, $K_{\theta b}(\theta)$ can be approximated by the product of the transversal and longitudinal incidence angle modifiers according to McIntire [18]:

$$K_{\theta b}(\theta) \equiv K_{\theta b}(\theta_l,\theta_t) \approx K_{\theta b,\,long}(\theta_l,0)K_{\theta b,\,trans}(0,\theta_t) \quad (6)$$

From Eqs. (3) and (5), the collector outlet temperature is calculated using the following equation:

$$\frac{q_u}{A_a} = \eta_0K_{\theta b}(\theta)G_b + \eta_0K_{\theta d}G_d - c_1(T_m-T_a) - c_2(T_m-T_a)^2 - c_3\frac{dT_m}{dt} \quad (7)$$

2.3. Plate heat exchanger

With the inlet temperatures of the plate heat exchanger in primary and secondary circuits, both the outlet temperatures are determined by the effectiveness-number of transfer units (NTU) method. The plate heat exchanger being used is of the unmixed counterflow configuration. The effectiveness can be expressed as a function of the number of transfer units, the heat capacity ratio, and the flow arrangement [19],

$$\varepsilon = \frac{\exp[(1-C^*)\mathrm{NTU}]-1}{\exp[(1-C^*)\mathrm{NTU}]-C^*} \quad (8)$$

with the number of transfer units it is defined as:

$$\mathrm{NTU} = \frac{U_{HX}A_{HX}}{C_{min}} \quad (9)$$

and the dimensionless heat capacity rate ratio,

$$C^* = \frac{C_{min}}{C_{max}} \quad (10)$$

where C_{min}/C_{max} is equal to C_c/C_h or C_h/C_c, depending on the relative magnitude of the hot and cold fluid heat capacity rates in primary and secondary circuits.

The overall heat transfer coefficient across a plate is defined as:

$$\frac{1}{U_{HX}} = \frac{1}{h_c} + \frac{1}{h_h} + \frac{t}{k_p} + R_{fc} + R_{fh} \tag{11}$$

where the heat transfer coefficients for both sides of the plate heat exchanger are calculated from the following correlations [20]:

$$\mathrm{Nu} = \frac{h_i D_e}{k_w} = C_h \mathrm{Re}^a \mathrm{Pr}^{1/3} = C_h \left(\frac{G_{ch} D_e}{\mu}\right)^a \left(\frac{\mu c_p}{k_w}\right)^{1/3} \quad \text{for } i = \mathrm{c, h} \tag{12}$$

where the values of C_h and a depend on the flow characteristics and chevron angle as given in Kumar [20] and the viscosity correction factor is ignored. This term is evaluated at the corresponding fluid mean temperature in the plate heat exchanger.

Once the effectiveness value is given from Eq. (8), both the outlet temperatures are obtained from the following effectiveness expression, defined as the ratio of the actual heat transfer rate for a heat exchanger to the maximum possible heat transfer rate,

$$\varepsilon = \frac{C_c(T_{c,o} - T_{c,i})}{C_{min}(T_{c,o} - T_{h,i})} = \frac{C_h(T_{h,o} - T_{h,i})}{C_{min}(T_{c,o} - T_{h,i})} \tag{13}$$

The total heat transfer area of the plate heat exchanger is designed according to the maximum heat load required. The collector area and the mass flow in the collector lead to this value. That means the heat exchanger has to be able to transfer the generated heat at maximum irradiance of the collector to the storage tank. The total heat transfer area is then calculated by the following equation:

$$A_{HX} = \frac{G_{T,max}\eta_0 A_c}{U_{HX}\mathrm{LMTD}} \tag{14}$$

It is obtained by a trial-and-error calculation procedure, which is accomplished by assuming the values of the overall heat transfer coefficient until the assumed and calculated values are in close agreement.

2.4. Storage tank

A mathematical model for heat transfer in the storage tank is based on the one-dimensional transient heat transport equation by convection and conduction along the prevailing flow direction of the storage tank. The multi-node model for the storage tank is employed to simulate the thermal stratification by dividing the tank into a specified number of tank segments. The longitudinal axis of the storage tank is assumed to be made up of N-disk shaped control volumes, each one having a uniform temperature. By considering the energy balance, which takes into account the convective and diffusive fluxes as well as the heat losses to the ambient within each control volume, a set of finite differential equations is established. The finite differential equation for the control volume j of the storage tank i gives:

$$\begin{aligned}
\rho_{i,j} c_{p,i,j} V_{i,j} \frac{T_{i,j} - T_{i,j}^n}{\Delta t} &= Q_{\mathrm{conv,in}}^{i,j} - Q_{\mathrm{conv,out}}^{i,j} + Q_{\mathrm{cond,in}}^{i,j} - Q_{\mathrm{cond,out}}^{i,j} - Q_{\mathrm{loss}}^{i,j} \\
&= \left\{ \begin{array}{ll} \dot{m}_l c_{p,i,j+1} T_{i,j+1}, & i < j \\ \left\{ \begin{array}{ll} \left(\dot{m}_s - \dot{m}_l\right) c_{p,i,j-1} T_{i,j-1}, & \dot{m}_s > \dot{m}_l \\ \left(\dot{m}_l - \dot{m}_s\right) c_{p,i,j+1} T_{i,j+1}, & \dot{m}_s < \dot{m}_l \end{array} \right\}, & j \le i \le k \end{array} \right\}, \; j \le k \\
&\quad \left\{ \begin{array}{ll} \dot{m}_s c_{p,i,j-1} T_{i,j-1}, & i > k \end{array} \right\} \\
&\quad \left\{ \begin{array}{ll} \dot{m}_l c_{p,i,j+1} T_{i,j+1}, & i \le k \\ 0, & k < i < j \\ \dot{m}_s c_{p,i,j-1} T_{i,j-1}, & i \ge j \end{array} \right\}, \; j > k \\
&\quad - \left\{ \begin{array}{ll} \dot{m}_l c_{p,i,j} T_{i,j}, & i \le j \\ \left\{ \begin{array}{ll} \left(\dot{m}_s - \dot{m}_l\right) c_{p,i,j} T_{i,j}, & \dot{m}_s > \dot{m}_l \\ \left(\dot{m}_l - \dot{m}_s\right) c_{p,i,j} T_{i,j}, & \dot{m}_s < \dot{m}_l \end{array} \right\}, & j \le i \le k \end{array} \right\}, \; j \le k \\
&\quad \left\{ \begin{array}{ll} \dot{m}_s c_{p,i,j} T_{i,j}, & i > k \end{array} \right\} \\
&\quad - \left\{ \begin{array}{ll} \dot{m}_l c_{p,i,j} T_{t,i,j}, & i \le k \\ 0, & k < i < j \\ \dot{m}_s c_{p,i,j} T_{i,j}, & i \ge j \end{array} \right\}, \; j > k \\
&\quad - kA_{cs} \frac{T_{i,j} - T_{i,j-1}}{\Delta h} + kA_{cs} \frac{T_{i,j+1} - T_{i,j}}{\Delta h} - U_t A_l \left(T_{i,j} - T_a\right)
\end{aligned} \tag{15}$$

where Δt is the time step, Δh is the grid spacing, and n denote the value at the previous time step.

The finite differential equations for the control volumes at the top ($j = 1$) and at the bottom ($j = N$) of the storage tanks are different to the finite differential Eq. (15) for the internal control volumes because of the perturbation occurring at the ends of the tank due to inflow and outflow at each end. Therefore, it is assumed that any incoming mass of cold or hot water is fully mixed at the location of the inlet. The finite differential equations for the control volumes at the top and bottom of the tank i are expressed as, respectively:

$$\rho_{i,j}c_{\mathrm{p},i,j}V_{i,j}\frac{T_{i,j}-T_{i,j}^{n}}{\Delta t}=Q_{\mathrm{conv}}^{i,1}+Q_{\mathrm{coll}}^{i,1}+Q_{\mathrm{net}}^{i,1}-Q_{\mathrm{cond}}^{i,1}-Q_{\mathrm{loss}}^{i,1}$$

$$=\left\{\begin{array}{l}\left\{\begin{array}{ll}\dot{m}_{\mathrm{l}}c_{\mathrm{p},i,2}T_{i,2}, & i<j\\ \left\{\begin{array}{ll}-\left(\dot{m}_{\mathrm{s}}-\dot{m}_{\mathrm{l}}\right)c_{\mathrm{p},i,1}T_{i,1}, & \dot{m}_{\mathrm{s}}>\dot{m}_{\mathrm{l}}\\ \left(\dot{m}_{\mathrm{l}}-\dot{m}_{\mathrm{s}}\right)c_{\mathrm{p},i,2}T_{i,2}, & \dot{m}_{\mathrm{s}}<\dot{m}_{\mathrm{l}}\end{array}\right\}, & j\le i\le k\\ -\dot{m}_{\mathrm{s}}c_{\mathrm{p},i,1}T_{i,1}, & i>k\end{array}\right\}, j\le k\\ \left\{\begin{array}{ll}\dot{m}_{\mathrm{l}}c_{\mathrm{p},i,2}T_{i,2}, & i\le k\\ 0, & k<i<j\\ -\dot{m}_{\mathrm{s}}c_{\mathrm{p},i,1}T_{i,1}, & i\ge j\end{array}\right\}, j>k\end{array}\right\}$$

$$+F_i^{\mathrm{c}}\dot{m}_{\mathrm{s}}c_{\mathrm{p,h}}T_{\mathrm{h,o}}+\left\{\begin{array}{l}\left\{\begin{array}{ll}\dot{m}_{\mathrm{m},i}c_{\mathrm{p},i,1}T_{i,1}, & \dot{m}_{\mathrm{m},i}\le 0\\ \dot{m}_{\mathrm{m},i}c_{\mathrm{p},i-1,N}T_{i-1,N}, & \dot{m}_{\mathrm{m},i}\ge 0\end{array}\right\}, i\ne 1\\ -\dot{m}_{\mathrm{l}}c_{\mathrm{p},i,1}T_{i,1}, \quad i=1\end{array}\right\}$$

$$+kA_{\mathrm{cs}}\frac{T_{i,2}-T_{i,1}}{\Delta h}-U_{\mathrm{t}}\left(A_{\mathrm{cs}}+A_{\mathrm{l}}\right)\left(T_{i,1}-T_{\mathrm{a}}\right) \tag{16}$$

$$\rho_{i,N}c_{\mathrm{p},i,N}V_{i,N}\frac{T_{i,N}-T_{i,N}^{n}}{\Delta t}=Q_{\mathrm{conv}}^{i,N}+Q_{\mathrm{load}}^{i,N}+Q_{\mathrm{net}}^{i,N}+Q_{\mathrm{cond}}^{i,N}-Q_{\mathrm{loss}}^{i,N}$$

$$=\left\{\begin{array}{l}\left\{\begin{array}{ll}-\dot{m}_{\mathrm{l}}c_{\mathrm{p},i,N}T_{i,N}, & i<j\\ \left\{\begin{array}{ll}\left(\dot{m}_{\mathrm{s}}-\dot{m}_{\mathrm{l}}\right)c_{\mathrm{p},i,N-1}T_{i,N-1}, & \dot{m}_{\mathrm{s}}>\dot{m}_{\mathrm{l}}\\ -\left(\dot{m}_{\mathrm{l}}-\dot{m}_{\mathrm{s}}\right)c_{\mathrm{p},i,N}T_{i,N}, & \dot{m}_{\mathrm{s}}<\dot{m}_{\mathrm{l}}\end{array}\right\}, & j\le i\le k\\ \dot{m}_{\mathrm{l}}c_{\mathrm{p},i,N-1}T_{i,N-1}, & i>k\end{array}\right\}, j\le k\\ \left\{\begin{array}{ll}-\dot{m}_{\mathrm{l}}c_{\mathrm{p},i,N}T_{i,N}, & i\le k\\ 0, & k<i<j\\ \dot{m}_{\mathrm{s}}c_{\mathrm{p},i,N-1}T_{i,N-1}, & i\ge j\end{array}\right\}, j>k\end{array}\right\}$$

$$+F_i^{\mathrm{l}}\dot{m}_{\mathrm{l}}c_{\mathrm{p,r}}T_{\mathrm{r}}+\left\{\begin{array}{l}\left\{\begin{array}{ll}\dot{m}_{\mathrm{m},i+1}c_{\mathrm{p},i+1,1}T_{i+1,1}, & \dot{m}_{\mathrm{m},i+1}\le 0\\ -\dot{m}_{\mathrm{m},i+1}c_{\mathrm{p},i,N}T_{i,N}, & \dot{m}_{\mathrm{m},i+1}\ge 0\end{array}\right\}, i\ne 4\\ -\dot{m}_{\mathrm{s}}c_{\mathrm{p},i,N}T_{i,N}, \quad i=4\end{array}\right\}$$

$$-kA_{\mathrm{cs}}\frac{T_{i,N}-T_{i,N-1}}{\Delta h}-U_{\mathrm{t}}\left(A_{\mathrm{cs}}+A_{\mathrm{l}}\right)\left(T_{i,N}-T_{\mathrm{a}}\right) \tag{17}$$

where a control function F_i^{c} that determines to which storage tank receives water from the heat exchanger is written as follows:

$$F_i^{\mathrm{c}}=\begin{cases}1, & \text{if } T_{\mathrm{h,o}}>T_{i,1},\ i=1\\ 1, & \text{if } T_{i-1,1}\geqslant T_{\mathrm{h,o}}>T_{i,1},\ i=2,3,4\\ 1, & \text{if } T_{\mathrm{h,o}}\leqslant T_{i,1},\ i=4\\ 0, & \text{otherwise}\end{cases} \tag{18}$$

The water returning from the load is controlled in a similar manner with a load return control function F_i^{l}:

$$F_i^{\mathrm{l}}=\begin{cases}1, & \text{if } T_{\mathrm{r}}>T_{i,N},\ i=1\\ 1, & \text{if } T_{i-1,N}\geqslant T_{\mathrm{r}}>T_{i,N},\ i=2,3,4\\ 1, & \text{if } T_{\mathrm{r}}\leqslant T_{i,N},\ i=4\\ 0, & \text{otherwise}\end{cases} \tag{19}$$

The net flow between storage tanks depends on the magnitudes of the collector and load flow rates and the values of the control functions at any particular instant, and it can be determined with function F_i'.

$$F_i'=\begin{cases}\dot{m}_{\mathrm{m},1}=0\\ \dot{m}_{\mathrm{m},i}=\dot{m}_{\mathrm{c}}\sum_{j=1}^{i-1}F_j^{\mathrm{c}}-\dot{m}_{\mathrm{l}}\sum_{j=1}^{N}F_j^{\mathrm{l}}\\ \dot{m}_{\mathrm{m},N+1}=0\end{cases} \tag{20}$$

Energy demand met by solar energy is calculated as,

$$q_{\mathrm{s}}=\dot{m}_{\mathrm{l}}c_{\mathrm{p,tr}}(T_{\mathrm{t}}-T_{\mathrm{r}}) \tag{21}$$

When $T_{\mathrm{t}}<T_{\mathrm{l}}$, the desired load temperature requirement can be met by an auxiliary energy. The required auxiliary energy is calculated as,

$$q_{\mathrm{a}}=\dot{m}_{\mathrm{l}}c_{\mathrm{p,lt}}(T_{\mathrm{l}}-T_{\mathrm{t}}) \tag{22}$$

The annual thermal performance of the plant, characterized by annual collector efficiency and solar fraction, is defined as:

$$\mathrm{SE}=\frac{Q_{\mathrm{u}}}{Q_{\mathrm{r}}}=\frac{\sum\int_0^t q_{\mathrm{u}}\mathrm{d}t}{N_{\mathrm{c}}A_{\mathrm{a}}\sum\int_0^t I_{\mathrm{T}}\mathrm{d}t} \tag{23}$$

$$\mathrm{SF}=\frac{Q_{\mathrm{s}}}{Q_{\mathrm{s}}+Q_{\mathrm{a}}}=\frac{\sum\int_0^t q_{\mathrm{s}}\mathrm{d}t}{\sum\int_0^t q_{\mathrm{s}}\mathrm{d}t+\sum\int_0^t q_{\mathrm{a}}\mathrm{d}t} \tag{24}$$

2.5. Multi effect distillation

A numerical model is developed using mass, concentration, and energy balances of the major components in the MED system with a backward-feed configuration. The mass balance equation for the transient seawater inventory in the evaporator side of the system is given as,

$$\frac{dm_e}{dt} = \dot{m}_f - \dot{m}_b - \dot{m}_v \tag{25}$$

Here m_e is the mass of seawater in the evaporator side, $\dot{m}_f$ is the feed water flow rate, $\dot{m}_b$ and $\dot{m}_v$ are the brine and vapor flow rates leaving the effect. The seawater concentration in each effect is calculated as,

$$\frac{d(m_e X_e)}{dt} = \dot{m}_f X_f - \dot{m}_b X_e - \dot{m}_v X_v \tag{26}$$

where X is the total dissolved solids (TDS) in parts per million (ppm) and the TDS of the distillate is taken as 10 ppm.

The energy balance for the evaporator side of each effect can be written as,

$$\frac{d(\dot{m}_e u_e)}{dt} = \overbrace{\dot{m}_f h_f(T_f)}^{\text{Feed}} - \overbrace{\dot{m}_b h_f(T_b)}^{\text{Brine discharge}} - \overbrace{\dot{m}_v h_{fg}(T_v)}^{\text{Vapor}} + \overbrace{h_o A_o (T_t - T_o)}^{\text{Heat transfer}} \tag{27}$$

The present design adopts the falling film evaporation of seawater over a bundle of horizontal tubes. The Han and Fletcher's correlation [21] is applied for the boiling of seawater over circumferentially groove tubes and it is given as,

$$h_o \left(\frac{v^2}{k^3 g}\right)^{1/3} = 0.0007 \mathrm{Re}^{0.2} \mathrm{Pr}^{0.65} q''^{0.4} \tag{28}$$

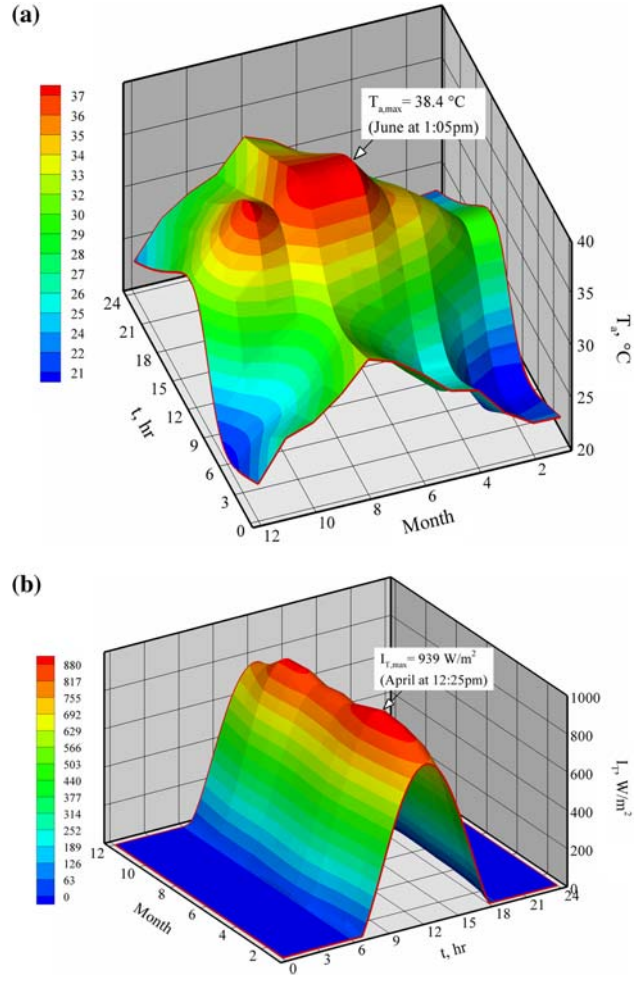

Fig. 3. Contour plots of (a) monthly average hourly ambient temperature and (b) global radiation on the tilted surface in Jeddah, Saudi Arabia.

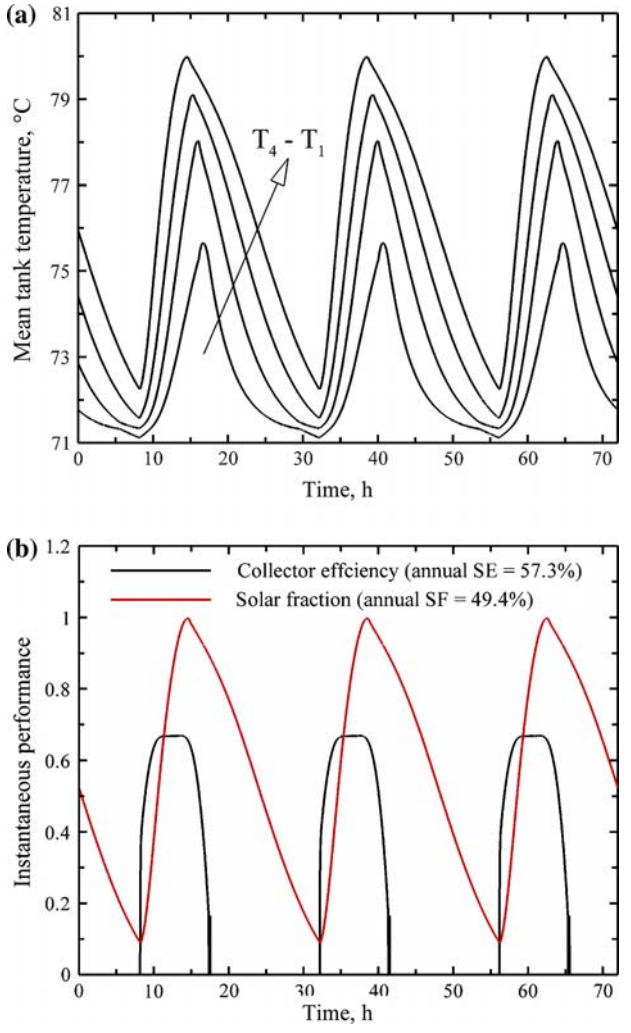

Fig. 4. The Mean tank temperature profiles of four storage tanks over the three days from April 14 to 15 for the heating water temperature of 80°C with A_c = 849 m^2 and V_t = 280 m^3: (a) mean tank temperature; (b) instantaneous collector efficiency and solar fraction.

The energy balance for the metal tubes is written as,

$$\rho c_p V \frac{dT_t}{dt} = h_i A_i (T_h - T_t) - h_o A_o (T_t - T_o) \quad (29)$$

For the first effect, hot water is used and the energy balance is given as,

$$\rho c_p V \frac{dT_h}{dt} = \dot{m}(h_f(T_l) - h_f(T_r)) - h_i A_i (T_h - T_t) \quad (30)$$

The heat transfer coefficient for hot water inside the tube is calculated using Dittus–Boelter's correlation as,

$$Nu = 0.023\,Re^{0.8}Pr^{0.4} \quad (31)$$

Nusselt film condensation correlation is applied to calculate the heat transfer coefficient for condensation of the water vapor on the condenser tubes and it is given as,

$$h_i = 0.728\left[\frac{\rho_l g k^3 (\rho_l - \rho_v)\,[h_{fg} + \frac{3}{8}c_{pl}(T_h - T_t)]}{D\mu\,(T_h - T_t)}\right]^{0.25} \quad (32)$$

Finally, the overall heat transfer coefficient U_i is calculated as,

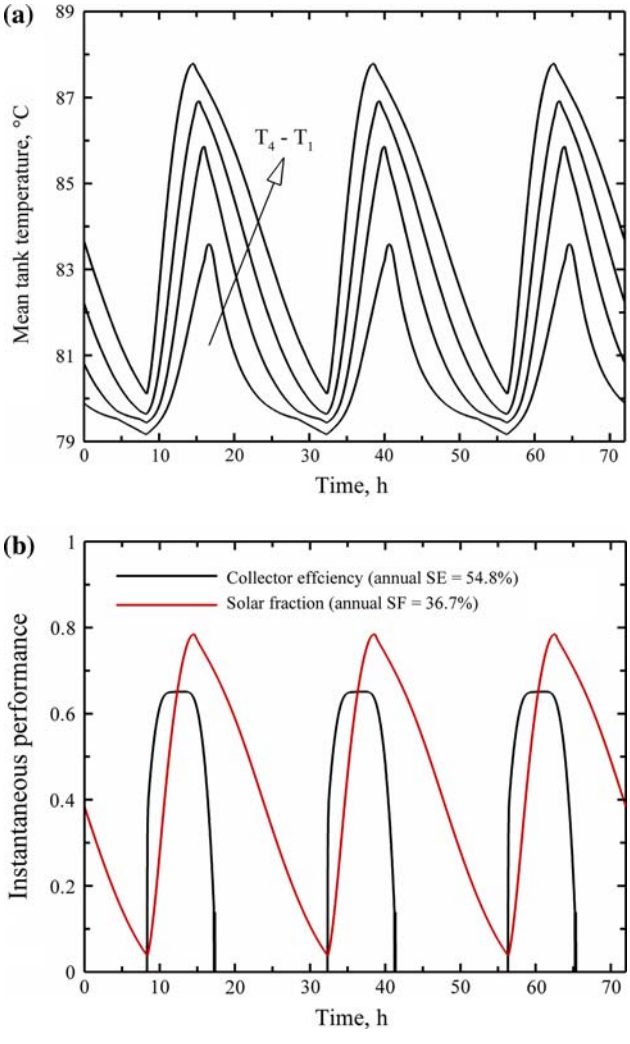

Fig. 5. The Mean tank temperature profiles of four storage tanks over the three days from April 14 to 15 for the heating water temperature of 90℃ with $A_c = 849$ m^2 and $V_t = 280$ m^3: (a) mean tank temperature; (b) instantaneous collector efficiency and solar fraction.

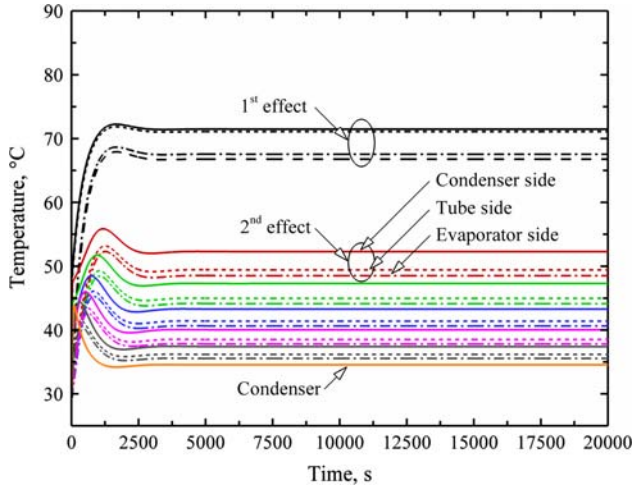

Fig. 6. Temporal temperature profiles of the SMED system for the heating water temperature of 80℃.

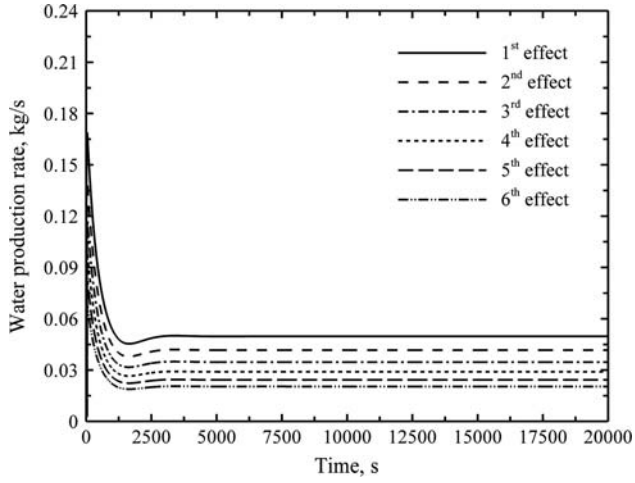

Fig. 7. The transient water production rate at each effect of the SMED system for the heating water temperature of 80℃.

$$U_{\mathrm{i}} = \left[\frac{1}{h_{\mathrm{i}}} + \frac{r_{\mathrm{i}}\, l\, n^{\frac{r_{\mathrm{o}}}{r_{\mathrm{i}}}}}{k} + \frac{A_{\mathrm{i}}}{A_{\mathrm{o}}}\frac{1}{h_{\mathrm{o}}}\right]^{-1} \tag{33}$$

The amount of water vapor produced in each effect ($\dot{m}_{\mathrm{w,i}}$) is obtained as,

$$\dot{m}_{\mathrm{w,i}} = \frac{U_i\, A_i\, \mathrm{LMTD_i}}{h_{\mathrm{fg}}(T_{\mathrm{i}})} \tag{34}$$

The overall water production rate (WPR) and the performance ratio (PR) by the plant are given as,

$$\mathrm{WPR} = \sum_{i=1}^{N} \dot{m}_{\mathrm{w,i}} \tag{35}$$

$$\mathrm{PR} = \frac{\sum_{i=1}^{N} \dot{m}_{\mathrm{w,i}}\, h_{\mathrm{fg}}(T_{\mathrm{i}})}{\dot{m}_{\mathrm{l}}\, c_{\mathrm{p}}(T_{\mathrm{h}})\,(T_{\mathrm{l}} - T_{\mathrm{r}})} \tag{36}$$

For the simulation of SMED system, the plant parameters and input data are shown in Table 2.

3. Results and discussion

The thermal and performance analyses of SMED system, which comprises 849 m^2 of evacuated-tube collectors, 280 m^3 water storage tanks, auxiliary heater, and six effects based on baseline configuration mentioned previously, are carried out with respect to heating water temperature in the range of 80–90°C. The system performances are reported in terms of the annual solar fraction and collector efficiency, as well as the overall water production rate and performance

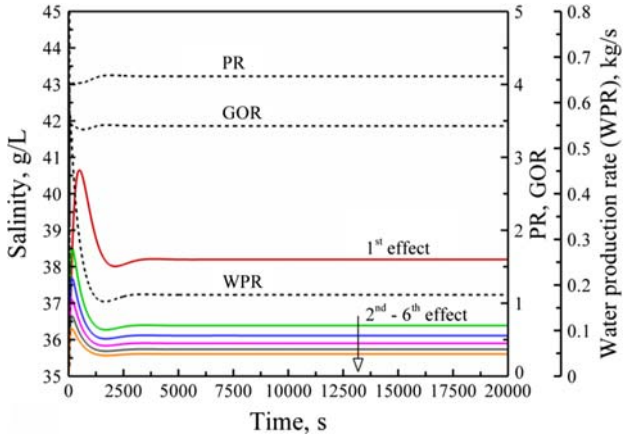

Fig. 8. The concentration, PR, GOR, and total WPR of the SMED system for the heating water temperature of 80°C.

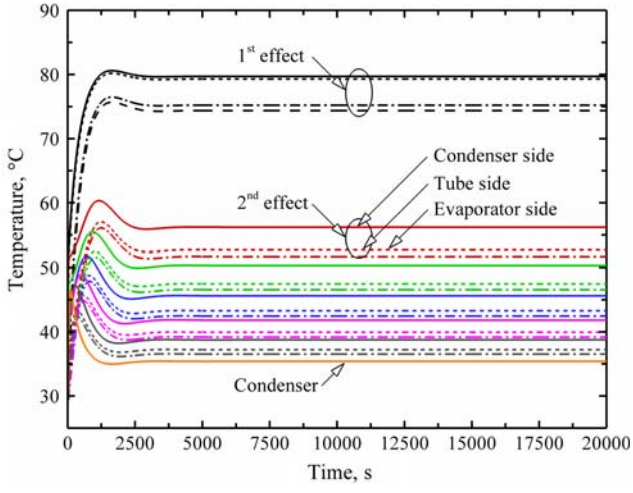

Fig. 9. Temporal temperature profiles of the SMED system for the heating water temperature of 90°C.

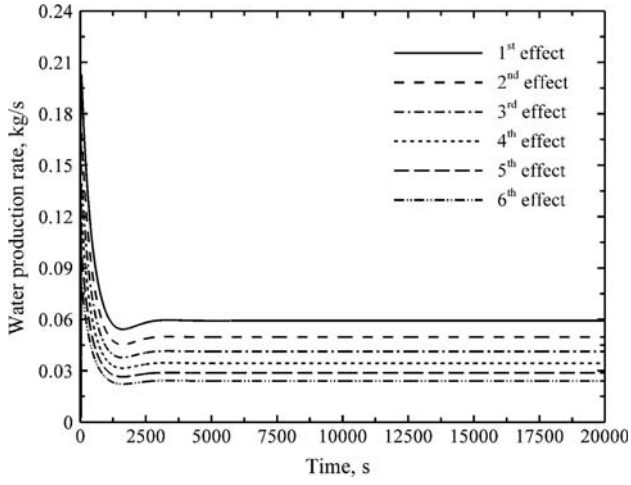

Fig. 10. The transient water production rate at each effect of the SMED system for the heating water temperature of 90°C.

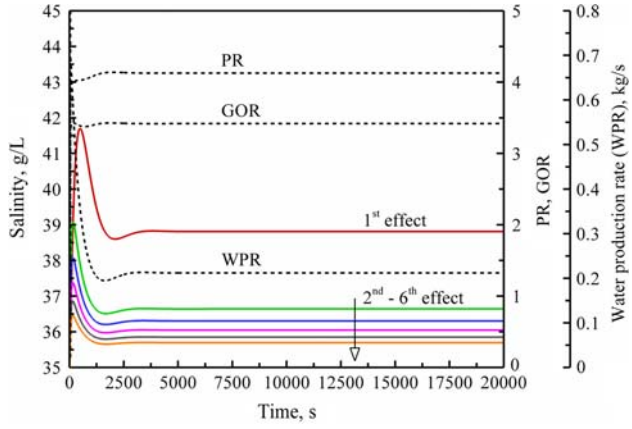

Fig. 11. The concentration, PR, GOR, and total WPR of the SMED system for the heating water temperature of 90°C.

ratio. For the simulations, Fig. 3 shows the monthly average hourly ambient temperature based on the measured data and the global radiation on the tilted surface obtained from the aforementioned solar radiation model. The maximum monthly average hourly ambient temperature and global radiation are about 38℃ in June and about 940 W/m^2 in April, respectively.

The mean temperature profiles of four storage tanks and the instantaneous solar fraction and collector efficiency of solar collector over the three days from April 14 to 15 for the heating water temperature of 80℃ are presented in Fig. 4. Here, the mean temperature of the storage tank i is calculated as,

$$T_i^{\mathrm{m}} = \frac{\sum_{j=1}^{N} \rho_{i,j} V_{i,j} T_{i,j}}{\sum_{j=1}^{N} \rho_{i,j} V_{i,j}} \tag{37}$$

As shown in Fig. 4a, the storage temperatures increase from about 8:30 am with increasing solar energy incident on the collector, and then decrease gradually until about 8:30 am next day after attaining a maximum value at about 2:30 pm, which is due to load demand and low solar energy. The effect of storage temperature is reflected on the instantaneous solar fraction shown in Fig. 4b. The annual collector efficiency and solar fraction are 57.3 and 49.4%. Fig. 5 presents the mean temperature profiles of four storage tanks and the instantaneous solar fraction and collector efficiency of solar collector over the three days from April 14 to 15 for the heating water temperature of 90℃. The annual collector efficiency and the solar fraction are 54.8 and 36.7%, respectively. For the heating water temperature of 85℃, these values are 56 and 42.4%.

A backward-feed counterflow multi-effect distillation system is adopted to be coupled with the solar hot water system. The MED system consists of six effects and a condenser. The hot water generated by the solar hot water system is used as the heat source for the evaporation of the seawater. The feed seawater is used for the condensation of the water vapor inside the condenser unit while part of the outlet seawater is used as make-up water. The make-up seawater is heated successively as it is pumped to the first effect by the condensation heat of the water vapor.

The temperature profiles of the each component in the SMED system for the heating water temperature of 80℃ are given in Fig. 6. It is noted that there is a substantial drop in the temperature between the first and the second effects due to quenching by the high flow rate of seawater supply. The temperature differ-

Table 3
Summary of the performance of SMED system at different heating water temperatures

Parameter	Heating water inlet and outlet temperatures, $T_1 - T_r$ (℃)									
	80 – 71.48℃			85 – 75.59℃			90 – 79.71℃			
	Condenser side (℃)	Tube side (℃)	Evaporator side (℃)	Condenser side (℃)	Tube side (℃)	Evaporator side (℃)	Condenser side (℃)	Tube side (℃)	Evaporator side (℃)	
1st effect	71.09	67.56	66.78	75.19	71.38	70.57	79.29	75.21	74.37	
2nd effect	52.29	49.43	48.52	54.27	51.08	50.13	56.21	52.70	51.70	
3rd effect	47.29	44.97	44.14	48.82	46.23	45.35	50.32	47.46	46.54	
4th effect	43.28	41.40	40.64	44.45	42.35	41.55	45.61	43.28	42.45	
5th effect	40.04	38.51	37.83	40.93	39.23	38.51	41.81	39.92	39.17	
6th effect	37.42	36.18	35.56	38.08	36.70	36.05	38.74	37.21	36.53	
Condenser		34.55			34.97			35.39		
WPR (kg/s)		0.179			0.195			0.212		
PR		4.11			4.12			4.13		
GOR		3.43			3.42			3.42		
Annual SE (%)		57.28			56.03			54.76		
Annual SF (%)		49.42			42.43			36.67		

ence between the effects is found to be around 2–5˚C. Fig. 7 shows the transient water production rate at each effect with the heating water temperature of 80˚ C. The first effect produces about 0.05 kg/s while that by the successive effects is reduced due to the thermal degradation yet the product rate by the first effect is followed. Fig. 8 depicts the concentration, the performance ratio, the gain output ratio, and the total water production rate of the SMED system for the heating water temperature of 80˚C. It is noted that the concentration of the seawater in the first effect is about 38,198 ppm (mg/L) in terms of total dissolved solids. The total WPR by the system is about 0.18 kg/s while the PR and the gain output ratio (GOR) are 4.11 and 3.43, respectively.

The temporal temperature profiles of each component in the system with the heat source at 90˚C are depicted in Fig. 9. It is observed that the temperature drop between the first and the second effects is greater than that of the heating water temperature of 80˚C. Fig. 10 represents the water production rate profiles at each effect. The first effect produces about 0.059 kg/s, while the production rate in the last effect is about 0.024 kg/s. The concentration, the performance ratio, the gain output ratio, and the total water production rate of the SMED system are illustrated in Fig. 11. It is shown that the concentration of the seawater in the first effect is about 38,810 ppm and the total water production rate is about 0.21 kg/s. The performance ratio and the gain output ratio are 4.13 and 3.42, respectively. It is noted that the MED cycle operation reaches steady-state condition 1 h after commencing the operation. The performance summary of the SMED plant operating at different heating water temperatures, i.e. 80, 85, and 90˚C, is furnished in Table 3.

4. Conclusions

A simulation model for predicting the transient behavior of a solar-assisted seawater desalination plant coupled with an evacuated-tube collector, with a multi-effect distillation system consisting of six effects and condenser with backward-feed configuration, has been presented. The thermal and performance analyses of SMED system, which comprises 849 m^2 of evacuated-tube collectors, 280 m^3 water storage tanks, auxiliary heater, and six effects based on baseline configuration mentioned previously, are carried out with respect to the heating water temperature in the range of 80–90˚C. The system performances are reported in terms of the annual solar fraction and collector efficiency, as well as the overall water production rate and performance ratio. As the heating water temperature increases from 80 to 90˚C, the annual collector efficiency and solar fraction decrease from 57.3 to 54.8% and from 49.4 to 36.7%, respectively. The total water production rate increases from 0.18 to 0.21 kg/s, while the performance ratio varies from 4.11 to 4.13 and the gain output ratio is about 3.4.

References

[1] K. Wangnick, in: Int. Workshop for small and medium size plants with limited environmental impact, Rome, 1998. Academia Nazionale delle Scienze detta Dei XL, 1999, pp. 41–57.
[2] K. Thu, A. Chakraborty, B.B. Saha, W.G. Chun, K.C. Ng, Life-cycle cost analysis of adsorption cycles for desalination, Desalin. Water Treat. 20 (2010) 1–10.
[3] K.C. Ng, K. Thu, G. Amy, M. Chunggaze, T.Y. Al-Ghasham, An advanced ADMED cycle for low-temperature driven desalination, US Provisional Application No. 61/450 (2011) 165.
[4] K. Thu, B.B. Saha, A. Chakraborty, K.C. Ng, Study on an advance adsorption desalination cycle with evaporator-condenser heat recovery circuit, Int. J. Heat Mass Transfer 54 (2011) 43–51.
[5] H. Lu, J.C. Walton, A.H.P. Swift, Desalination coupled to salinity gradient solar ponds, Desalination 136 (2001) 12–23.
[6] A.M. El-Nashar, Predicting part load performance of small MED evaporators—a simple simulation program and its experimental verification, Desalination 130 (2000) 217–234.
[7] E. Tzen, D. Theofilloyianakos, M. Sigalas, K. Karamanis, Design and development of a hybrid autonomous system for seawater desalination, Desalination 166 (2004) 267–274.
[8] P.W. Stackhouse, C.H. Whitlock, Surface meteorology and Solar Energy (SSE) rel. 6.0, NASA, 2010. http://eosweb.larc.nasa.gov/sse/.
[9] M. Collares-Pereira, A. Rabl, The average distribution of solar radiation-correlations between diffuse and hemispherical and between daily and hourly insolation values, Sol. Energy 22 (1979) 155–164.
[10] B.Y.H. Liu, R.C. Jordan, The interrelationship and characteristic distribution of direct, diffuse and total solar radiation, Sol. Energy 4 (1960) 119.
[11] J.E. Hay, J.A. Davies, Calculation of the solar radiation incident on an inclined surface, in: Proc. First Canadian Solar Radiation Data Workshop, 1980, pp. 59–72.
[12] R.C. Temps, K.L. Coulson, Solar radiation incident upon slopes of different orientations, Sol. Energy 19 (1977) 179–184.
[13] T.M. Klucher, Evaluation of models to predict insolation on tilted surfaces, Sol. Energy 23 (1979) 111–114.
[14] D.T. Reindl, W.A. Beckman, J.A. Duffie, Evaluation of hourly tilted surface radiation models, Sol. Energy 45 (1990) 917.
[15] Y.-D. Kim, K. Thu, H.K. Bhatia, C.S. Bhatia, K.C. Ng, Thermal analysis and performance optimization of a solar hot water plant with economic evaluation, Sol. Energy 86 (2012) 1378–1395.
[16] A. Rabl, Active Solar Collectors and their Applications, Oxford University Press, Oxford, 1985.
[17] EN 12975–2:2006. Thermal solar systems and components—Solar collectors—Part 2: Test Methods, Section 6.1. European Standard, March.
[18] W.R. McIntire, Factored approximations for biaxial incident angle modifiers, Sol. Energy 29 (1982) 315–322.
[19] R.P. Singh, D.R. Heldman, Introduction to Food Engineering, Elsevier, London, 2008.
[20] H. Kumar, The plate heat exchanger: construction and design, in: Proc. first UK National Conference on Heat Transfer, 1984, pp. 1275–1288.
[21] J. Han, L. Fletcher, Falling film evaporation and boiling in circumferential and axial grooves on horizontal tubes, Ind. Eng. Chem. Process Des. Dev. 24 (1985) 570–597.